

# An EV/PHEV Battery Charger Based on Sinusoidal-Ripple-Current Charging-Discharging Technique for V2G Applications

Mahdi Bayati,  
Amirkabir University of Technology,  
Tehran, Iran  
Email: bayati.mahdi@aut.ac.ir

Mehrdad Abedi,  
Email: abedi@aut.ac.ir

Gevork B. Gharepetian    Peyman Karimyan  
Email: grptian@aut.ac.ir

**Abstract**—Sinusoidal-Ripple-Current (SRC) charging-discharging technique has distinct advantages compared to other techniques. The purpose of this paper is to design a bidirectional Battery Charger (BC) for an Electric Vehicle (EV) based on SRC technique. Sinusoidal current variations applied to the Li-ion battery in this technique negatively affect on the AC-side terminal of the BC, alternately change the output active power, power factor, and current of the AC-side terminal and therefore, worsen the power quality. On the other hand, the output active power and reactive power of the AC-side terminal ( $P_s$  and  $Q_s$ ) must be regulated at constant values without any variations when the EV participates in (Vehicle-to-Grid) V2G technology. Therefore, a particular topology has been introduced and then, a novel control strategy has been defined for the BC of the EV in order to resolve the power quality problem and regulate  $P_s$  and  $Q_s$  at constant values. Finally, the simulation results confirm the validation of the proposed BC.

**Index Terms**—Active and reactive power control, bidirectional battery charger, charging-discharging technique, sinusoidal-ripple-current, vehicle-to-grid (V2G)

## I. INTRODUCTION

Upgrading conventional distribution grids to MicroGrids (MGs) has been studied in the past few years. Electric Vehicles (EVs) and Plug-in Hybrid EVs (PHEVs) as one of the elements connected to the MGs, have drawn a great deal of attention, due to rising energy costs, concerns about fossil energy reserves, energy security, environmental and climate change issues and legislation, and growing consumer expectations [1]. Although a large number of PHEVs/EVs connected to the MG may lead to a huge threat to quality and stability of the power system, they have enough potential to be used as distributed energy storage units. The bidirectional active and reactive power transfer through bidirectional Battery Chargers (BCs) of EVs is referred as Vehicle-to-Grid (V2G) technology [1], [2]. Some possible services provided by this technology are: supply of peak power, supply of primary, secondary and tertiary frequency control, load leveling, and voltage regulation [3].

Intensive research efforts are being conducted to make such advanced technology a reality today. One of the essential steps to successfully implement V2G concept is to design appropriate bidirectional BCs for EVs whose control systems

regulate output active and reactive power of the AC-side terminal ( $P_s$  and  $Q_s$ ) at requested values [4]–[7]. This task will be accomplished in this paper.

On the other hand, degradation on the battery during V2G technology makes it inconvenient and less preferable unless the battery performance and lifetime are under warranty. Thus, the bidirectional BCs should be designed based on a high-quality charging-discharging technique in order to obtain better battery performance and improve the battery lifetime.

Due to light weight, high power density, low self-discharge rate, and high operating voltage, utilization of Li-ion batteries as energy storage units of EVs has aggressively proliferated. Until now, some charging techniques for Li-ion batteries such as Constant-Current (CC) [8]–[10], Constant-Current Constant-Voltage (CC-CV) [8]–[10], pulse current [8], [10], [11], Reflex [8], [12], and Sinusoidal-Ripple-Current (SRC) [13], [14] have been proposed. Also, some discharging techniques for these batteries such as CC, pulse current, and SRC have been proposed [13]. Each charging or discharging technique has advantages and disadvantages.

In [14], SRC charging technique for Li-ion batteries has been investigated. The AC-impedance analysis has been used to explore the frequency  $f_m$  at which the AC impedance obtains its minimum value [14]. In [14], it has been proved that an optimal charging performance can be obtained when the Li-ion battery is charged based on SRC charging technique with  $f_m$ . Experiments have been shown that the charging time, charging efficiency, maximum rising temperature, and lifetime of Li-ion batteries are improved about 17%, 1.9%, 45.8%, and 16.1%, respectively, as compared with conventional CC-CV charging technique.

In [13], SRC discharging technique for Li-ion batteries has been investigated and it has been proved that an optimal discharging performance can be obtained when the Li-ion battery is discharged based on this technique with  $f_m$ . Experiments have been shown that this technique improves the discharging capacity, discharging efficiency, and rising temperature of Li-ion batteries about 1.3%, 1.32%, and 41.9%, respectively, as compared with conventional CC discharging technique.

Since this method has big distinct advantages in compar-

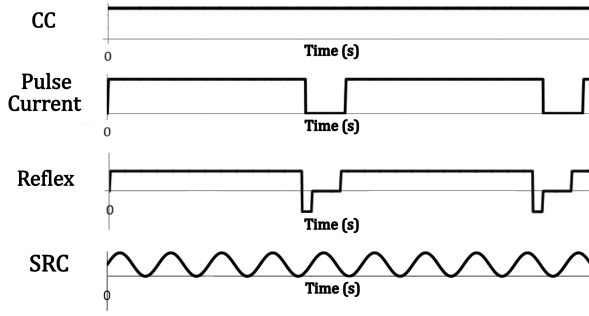


Fig. 1. Various types of charging-discharging battery current waveforms

ison with other charging and discharging techniques [13], [14], it has also been considered as a high quality charging-discharging technique in this research study. This charging-discharging technique can be used not only for EV BCs, but also for advanced battery systems.

As shown in Fig. 1, this technique applies a direct current ( $i_{DC}$ ) with an alternating sinusoidal current ( $i_{AC}$ ) with the frequency  $f_m$ . As a consequence of sinusoidal current variations applied to the Li-ion battery, the signal waveforms of delivered/extracted active powers to/from the Li-ion battery terminal and the AC-side terminal follow a sinusoidal shape. Such variations in  $P_s$  negatively affect on the AC-side terminal current, alternately change the Power Factor (PF) and the RMS value of the AC-side terminal current, and therefore, worsen the power quality. On the other hand,  $P_s$  and  $Q_s$  must be regulated at constant values without any variations when the EV participates in V2G technology. Thus, particular importance should be given to this power quality. Although this power quality has not been examined in details in the relevant studies conducted on SRC technique [13], [14], it has been investigated and solved in this paper.

The purpose of the study is to define a novel control strategy to resolve this power quality problem. For this purpose, a particular topology has been introduced in which one capacitor with two IGBT legs and two inductors are connected to the BC, and then are controlled according to the novel control strategy.

This work starts with a discussion about SRC technique in Section II. Then, Section III focuses on the model and control schemes of the DC-DC and DC-AC parts of the bidirectional BC based on SRC technique and finally, the paper will be concluded with relevant discussions on simulation results in Sections IV and V.

## II. SRC CHARGING-DISCHARGING TECHNIQUE

Fig. 2(a) depicts the complete AC-impedance model for the Li-ion battery which includes an ohmic resistance ( $R_o$ ), two double-layer capacitances ( $C_d'$  and  $C_d''$ ), two charge transfer resistances ( $R_{ct}'$  and  $R_{ct}''$ ), two inductances ( $L_d'$  and  $L_d''$ ), and two Warburg impedances ( $Z_w'$  and  $Z_w''$ ) [13], [14]. This circuit model can be simplified to the circuit model shown in Fig. 2(b) [13], [14]. The AC impedance for the Li-ion battery

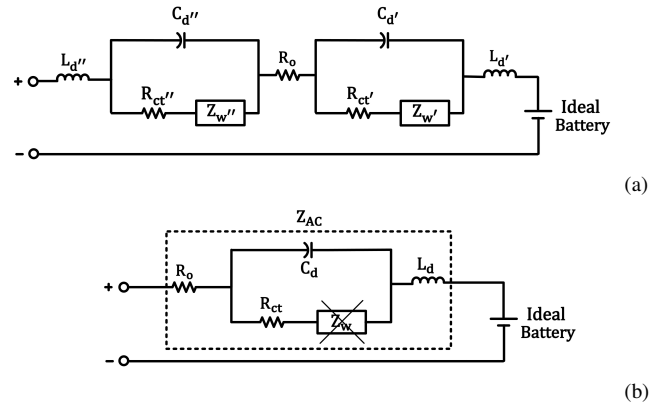


Fig. 2. Li-ion battery AC-impedance model: a) complete model and b) simplified model

is not affected by Warburg impedances only if the charging-discharging frequency is below 1Hz [13], [14]. If the charging-discharging technique is not CC, Warburg impedances can be neglected. Thus, the circuit model can be simplified again.

At the viewpoint of electrical circuit, different charging and discharging frequencies ( $f_c = \omega_c/(2\pi)$ ) result in different AC impedances. To have the minimum AC impedance ( $Z_{min}$ ), and as a result, the maximum energy transfer efficiency, the minimum energy loss, and finally, the best electrochemical reaction in both charging and discharging,  $f_c$  must be selected as follows [13], [14]:

$$f_c = f_m = \frac{1}{2\pi R_{ct} C_d} \sqrt{k-1} \quad (1)$$

where

$$k = \frac{\sqrt{2R_o R_{ct}^3 C_d^2 + 2L_d R_{ct}^2 C_d + R_{ct}^4 C_d^2}}{L_d} \quad (2)$$

The applied charging-discharging current can be written as: [13], [14]

$$i_{SRC} = i_{DC} + i_{AC} = I_0 + I_0 \cos(2\pi f_m t) \quad (3)$$

In the experiments conducted on the AC-impedance spectra of Li-ion batteries [13], [14], it has been revealed that  $f_m$  and  $|Z|_{min}$  vary for different Li-ion batteries and vary as a consequence of temperature and State of Charge (SOC) [13], [14]. Therefore, the designer faces a great serious challenge. This challenge is how to find  $f_m$  for a specific Li-ion battery pack with a specific SOC at a specific temperature in extensive use. Thus, it is worth to study and develop an online adaptive tuning algorithm, which is able to explore  $f_m$ , in the future. It has been shown that  $f_m$  for different Li-ion batteries are commonly within 900 to 1200 Hz [13], [14].  $f_m$  can be considered as a constant value to obtain a near-optimal charging-discharging performance [13], [14].

## III. MODELLING AND CONTROL SCHEME

Fig. 3 depicts the most common three-phase conductive configuration of EV/PHEV battery chargers [15]–[18]. Fig. 4

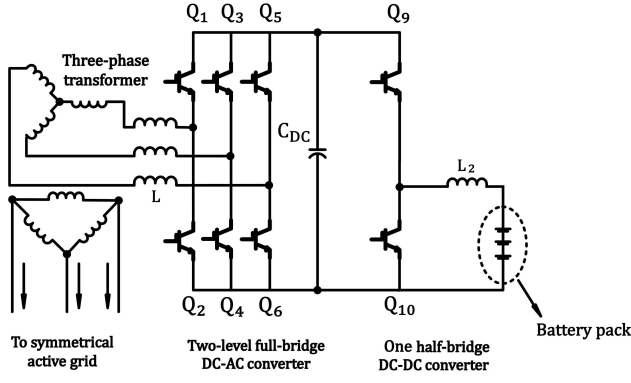


Fig. 3. A conventional topology for the EV bidirectional BC

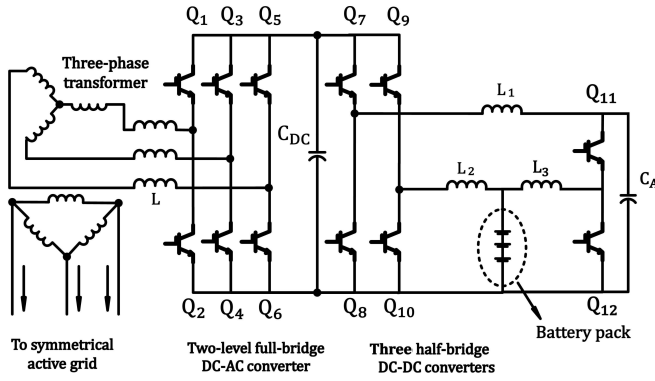
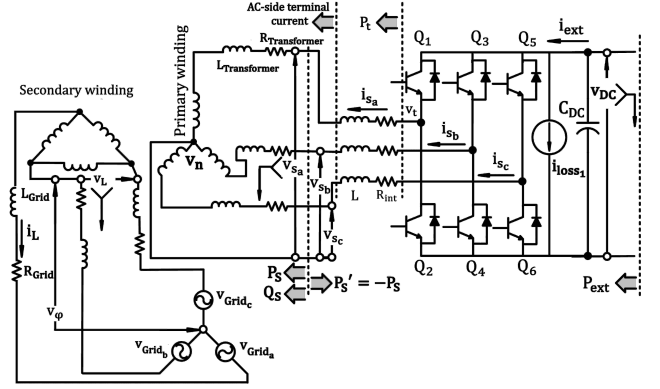


Fig. 4. Proposed topology for the EV bidirectional BC

proposes a particular configuration whose control system has been explained in this paper. It is preferred to have a part of the proposed system outside of the vehicle (off-board) [2] due to the relatively high power level, relatively heaviness and lack of space. It consists of a DC-DC part and a DC-AC part. The model and control of these parts will be explained in the following:

#### A. DC-AC Part

Fig. 5(a) shows the model of the DC-AC part. This part consists of whole the elements shown in the left side of the DC link capacitor in Fig. 4. Non-ideal characteristics of the switches impact on the design of controllers. To tackle this issue, the switching losses corresponding to each IGBT leg caused by the tailing current and reverse recovery current are modelled by a current source, connected in parallel with the DC link capacitor, whose amplitude is equal to  $Q_{rr} + Q_{tc}/T_s$  [19].  $Q_{rr}$ ,  $Q_{tc}$ , and  $T_s$  are the reverse recovery electric charge of one IGBT, tailing electric charge of one IGBT, and the switching period, respectively. Since there are three legs in this part, the amplitude of the current source is equal to [19]:

$$i_{loss1} = 3 \frac{Q_{rr} + Q_{tc}}{T_s} \quad (4)$$

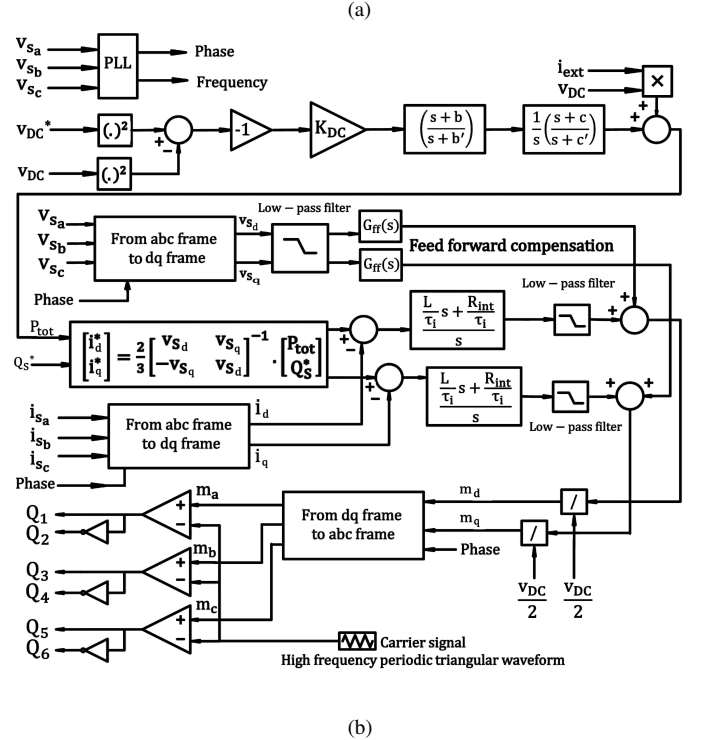


Fig. 5. DC-AC part: a) model and b) control system

The conduction losses corresponding to each IGBT leg caused by the internal resistance of the switches and inductors are modelled by the resistance  $R_{int}$  connected in series with each AC-side terminal [19].

The control system of the DC-AC part has been depicted in Fig. 5(b). First, the control system transforms the three-phase current  $i_s$  and voltage  $v_s$  from  $abc$  frame to  $dq$  frame. Moreover, there is a PLL to find the instantaneous phase and frequency of the applied three-phase voltage. It also includes two current control loops which receive the  $dq$  current references ( $i_{dref}$  and  $i_{qref}$ ) and suggest the  $abc$  modulating signals ( $m_a$ ,  $m_b$ , and  $m_c$ ) transformed from  $dq$  frame. To make the current control loops independently of  $v_{DC}$ , they are divided by half of  $v_{DC}$  [19]. They are augmented by the feedforward compensation which has big distinct benefits [19].  $i_{dref}$  and  $i_{qref}$  are calculated by the matrix equation,

shown in Fig. 5(b), so that  $P_s$  and  $Q_s$  follow  $P_{tot}$  and  $Q_s^*$ , respectively. The DC link voltage control system aims to suggest  $P_{tot}$  in order to regulate  $v_{DC}$  at  $v_{DC}^*$  with considering  $P_{ext}$  ( $i_{ext} \times v_{DC}$ ) as a disturbance.  $P_{tot}$  becomes equal to  $P_{ext}$  when  $v_{DC}$  reaches its steady state condition ( $v_{DC}^*$ ). With neglecting the switching and conduction losses,  $P_s$  becomes equal to  $P_{ext}$  in steady state condition of  $v_{DC}$  [19].  $i_{ext} \times v_{DC}$  or  $P_{ext}$  is imposed by the DC-DC part. Therefore, to have control over  $P_s$  and regulate it at  $P_s^*$ , the control system of the DC-DC part is needed. It determines the battery current references so that  $P_{ext}$  becomes equal to  $P_s^*$  [19]. Positive  $P_s^*$  discharges the Li-ion battery pack, while negative  $P_s^*$  charges it based on SRC technique.

### B. DC-DC Part

Fig. 6(a) shows the model of the DC-DC part. This part consists of whole the elements shown in the right side of the DC link capacitor in Fig. 4. The switching and conduction losses corresponding to each IGBT leg are modelled, just as previously mentioned. So, we can write [19]:

$$i_{loss2} = 2 \frac{Q_{rr} + Q_{tc}}{T_s} \quad (5)$$

$$i_{loss3} = \frac{Q_{rr} + Q_{tc}}{T_s} \quad (6)$$

There are three IGBT legs in the DC-DC part. One of them ( $Q_7Q_8$ ) belongs to the capacitor  $C_A$  and two of them ( $Q_9Q_{10}$  and  $Q_{11}Q_{12}$ ) belong to the Li-ion battery pack modelled by the AC-impedance model.

According to Equation (3), the current of the Li-ion battery pack consists of two terms,  $i_{DC}$  and  $i_{AC}$ . Fig. 6(b) is the control system of the IGBT legs  $Q_9Q_{10}$  and  $Q_{11}Q_{12}$  which regulates the current of the corresponding inductor  $i$  at  $i_{ref}$ .  $i$  can be  $i_{AC}$  or  $i_{DC}$ .  $i_{ref}$  can be  $i_{AC}^*$ , or  $i_{DC}^*$ .  $i_{DC}$  and  $i_{AC}$  are controlled and imposed by the control system of Fig. 6(b) using the IGBT legs  $Q_9Q_{10}$  and  $Q_{11}Q_{12}$ , respectively.  $i_{AC}^*$ , or  $i_{DC}^*$  must be determined as follows in order to regulate  $P_s$  and  $P_{ext}$  at  $P_s^*$ :

$$i_{Bat}^* = i_{DC}^* + i_{AC}^* = \left( -P_s^*/v_{Bat} \right) + \left( -P_s^*/v_{Bat} \right) \cos(2\pi f_m t) \quad (7)$$

Thus, the absorbed active power is given by:

$$P_{Bat} = P_{DC} + P_{AC} = v_{Bat} \times i_{Bat}^* \left( -P_s^* \right) + \left( -P_s^* \right) \cos(2\pi f_m t) \quad (8)$$

Fig. 6(c) is the control system of the IGBT leg  $Q_7Q_8$ . It receives the filtered RMS value of  $v_A$  and regulates the RMS value of  $v_A$  at  $v_A^*$ .  $v_A^*$  must be greater than  $v_{Bat}$  and less than  $v_{DC}^*$ . This is due to the fact that an IGBT leg decreases the voltage level.

This control system with the topology proposed in Fig. 4 resolve the power quality problem and eliminate the negative effects of the sinusoidal variations in  $P_{Bat}$  and  $i_{AC}$ ; Because, the alternating active power in the second term of Equation (8) is supplied by only  $C_A$  and  $P_{ext}$  becomes equal to the

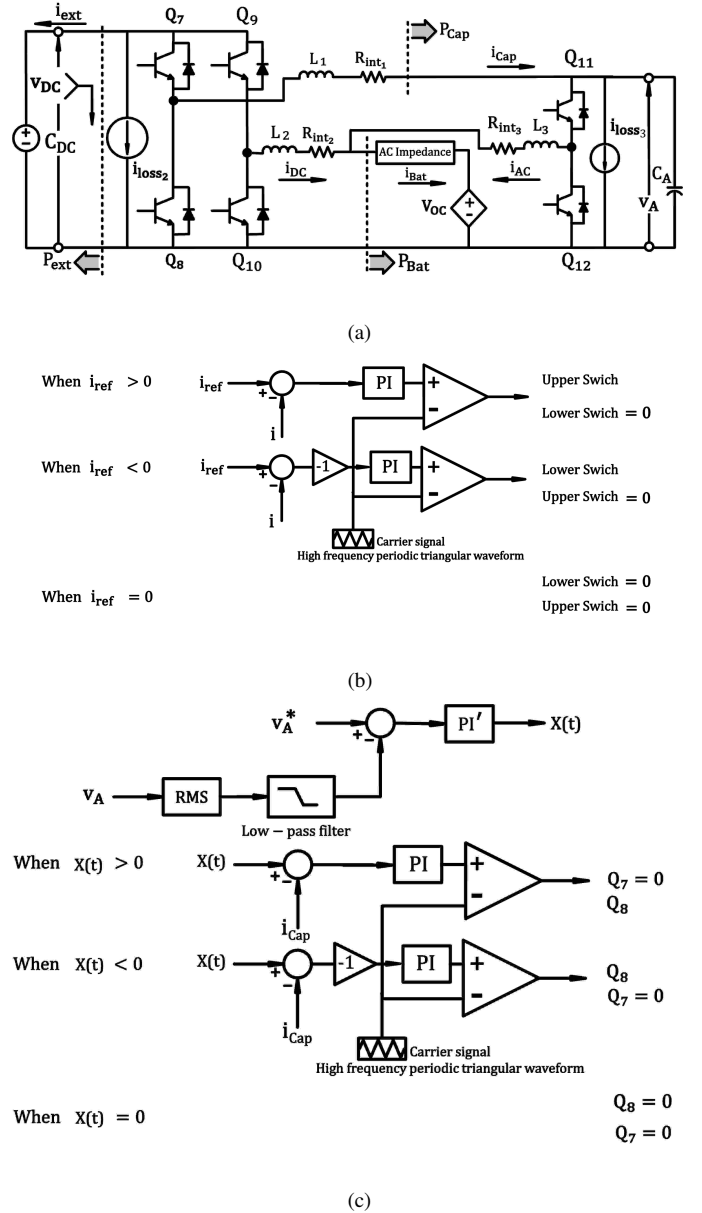


Fig. 6. DC-DC part: a) model, b) control system for the IGBT legs  $Q_9Q_{10}$  and  $Q_{11}Q_{12}$ , and c) control system for the IGBT leg  $Q_7Q_8$

first term of Equation (8). In other words, there are not sinusoidal variations in  $P_{ext}$  and  $P_s$ , and as a result, the AC-side terminal current has a sinusoidal waveform and its RMS value is not changed. If the topology in Fig. 3 is used,  $P_{AC}$  must be supplied by the power system. Thus,  $P_{ext}$  will have a sinusoidal term. This worsen the power quality of the AC-side terminal current. This matter has been indicated in Fig. 10.

## IV. SIMULATION RESULTS

The model and the control system of the bidirectional BC, which has already been explained in the form of DC-DC and DC-AC parts, are simulated by MATLAB/Simulink software with the parameters summarized in Appendix A.

$P_s^*$  is changed from -19.2 kW to 19.2 kW at  $t_0 = 0.6$  s.  $Q_s^*$  is changed from -10 kVAR to 10 kVAR at  $t_0 = 0.4$  s and then, is changed from 10 kVAR to -10 kVAR at  $t_0 = 0.8$  s.  $P_s^*$  and  $Q_s^*$  are independently set to validate the flexibility of the control system in switching among all the four quadrants of the  $P_s-Q_s$  plane. The positive  $P_s^*$  discharges the battery pack (after 0.6s), while the negative  $P_s^*$  charges it (before 0.6s) based on SRC technique as shown in Fig. 7. The signal waveforms in Fig. 7 are in agreement with Equations (7) and (8). Fig. 8 shows that the proposed BC is working under four different conditions within one second.

The capacitor  $C_A$  supplies  $P_{AC}$  and  $i_{AC}$ . The waveform of  $v_A$  has sinusoidal variations due to sinusoidal changes in  $i_{AC}$  and  $P_{AC}$ , as shown in Fig. 7(b) and 9(a). In spite of sinusoidal variations in  $v_A$ , applying  $i_{AC}^*$  does not change the RMS value of  $v_A$ ; Because the DC component (the mean value) of  $P_{AC}$  is equal to zero. But due to the switching losses caused by  $i_{loss3}$  and the conduction losses caused by  $R_{int3}$ , the RMS value of  $v_A$  decreases. Therefore, to maintain it at a constant value ( $v_A^*$ ), the IGBT leg  $Q_7Q_8$  has been used. The purpose of its control system is to keep the RMS value of  $v_A$  at 550V.

Fig. 10 compares two bidirectional BCs shown in Fig. 4 and Fig. 3. Fig. 10(a) corresponds to the AC-side terminal current of Fig. 4. Fig. 10(b) corresponds to the AC-side

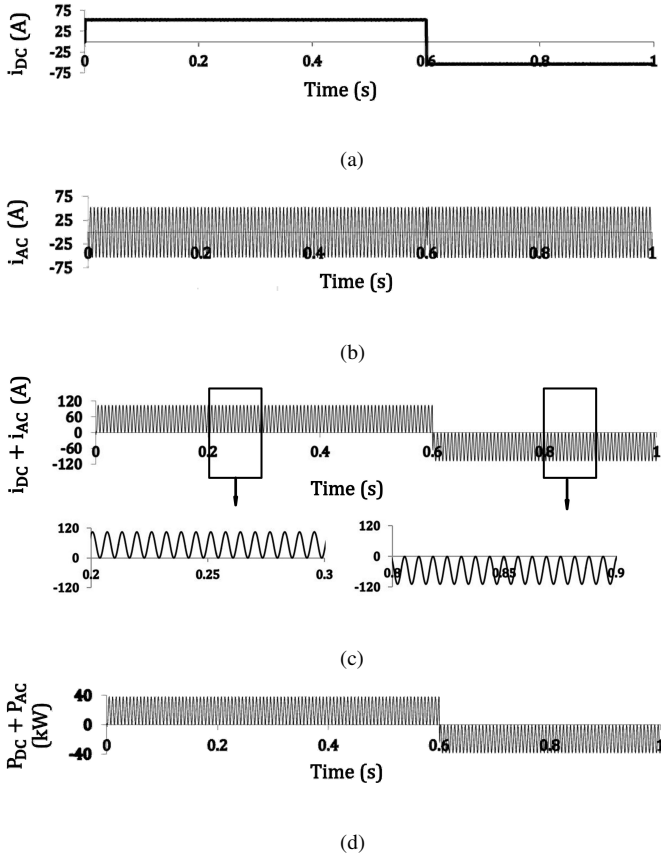


Fig. 7. Important signal waveforms of the battery pack of the BBC: a) DC component of the current, b) AC component of the current, c) summation of the AC and DC components of the current, and d) absorbed active power

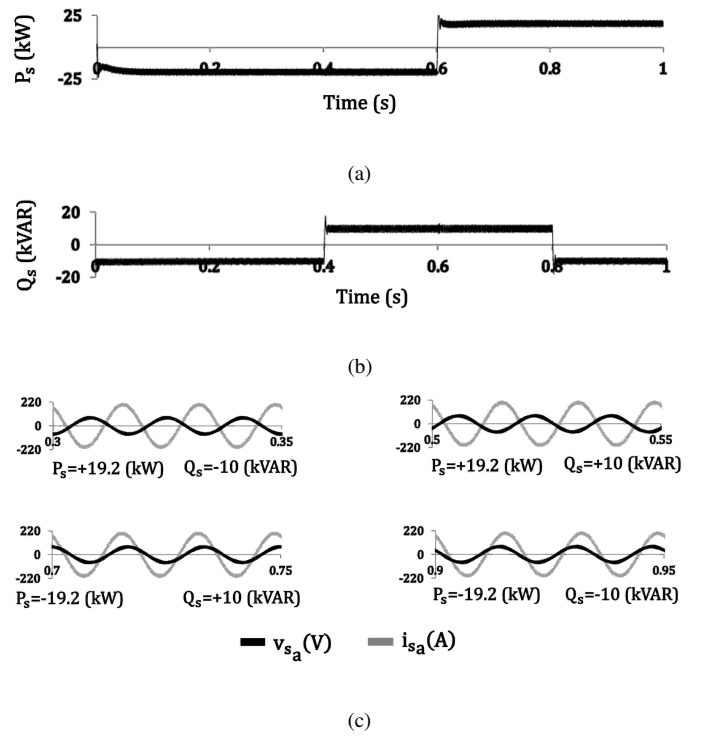


Fig. 8. Important signal waveforms of the AC-side terminal of the BBC: a) output active power, b) output reactive power, c) current and voltage

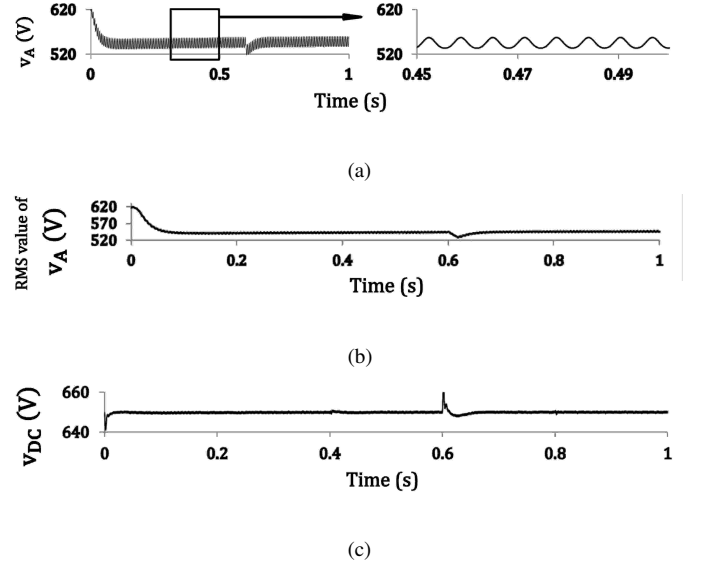


Fig. 9. a)  $v_A$ , b) RMS value of  $v_A$ , and c) DC link voltage

terminal current of Fig. 3. The simulation results prove that the proposed novel control strategy has resolved the mentioned power quality. The RMS value of the AC-side terminal current alternately changes for the conventional BC, while it is kept constant for the proposed BC.

## V. CONCLUSION

SRC charging-discharging technique has distinct advantages compared to other techniques. The purpose of this paper was to

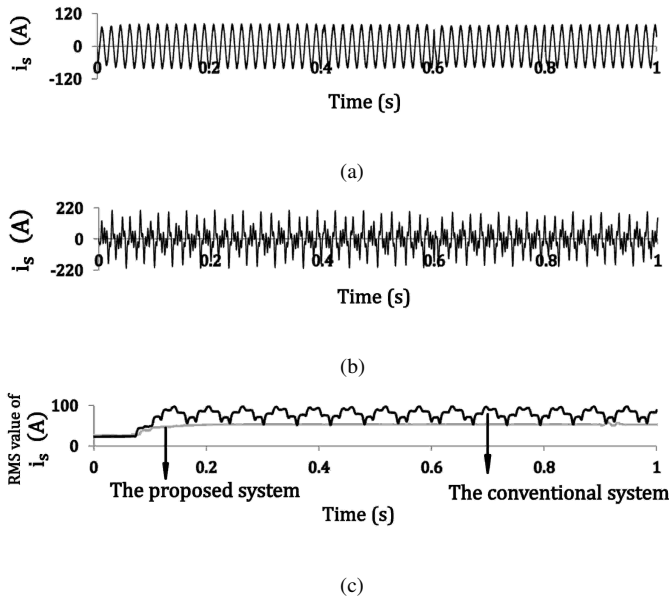


Fig. 10. Comparison of the proposed BBC and the conventional BBC: a) AC-side terminal current of the proposed BBC, b) AC-side terminal of the conventional BBC, and c) RMS value of these currents

design a bidirectional BC for an EV based on SRC technique. Sinusoidal current variations applied to the Li-ion battery in this technique negatively affect on the AC-side terminal of the BC, alternately change the output active power ( $P_s$ ), power factor, and current of the AC-side terminal and therefore, worsen the power quality. On the other hand,  $P_s$  and  $Q_s$  must be regulated at constant values without any variations when the EV participates in V2G technology. Therefore, a particular topology was introduced and then, a novel control strategy was defined for the BC of the EV in order to resolve the power quality problem and regulate  $P_s$  and  $Q_s$  at constant values. Finally, the simulation results confirmed that the effect of sinusoidal current variations has been eliminated and the proposed BC can adjust  $P_s$  and  $Q_s$  at desired values.

#### APPENDIX A SOME IMPORTANT PARAMETERS

$$\begin{aligned}
 [L \ L_1 \ L_2 \ L_3 \ L_G \ L_d] &= [4 \ 3.3 \ 3.3 \ 3.3 \ 0.08 \ 0.0014516] \text{ mH} \\
 [C_{DC} \ C_A \ C_d] &= [3 \ 3 \ 35.67] \text{ mF} \\
 [v_{OC} \ v_{DC}^* \ v_A^*] &= [360 \ 650 \ 550] \text{ V} \\
 [f_0 \ f_s \ f_m] &= [60 \ 3420 \ 992] \text{ Hz} \\
 [T_i] &= [0.5] \text{ ms} \\
 [R_G \ R_o \ R_{ct}] &= [0 \ 0.03615 \ 22.51] \text{ m}\Omega \\
 [R_{int} \ R_{int1} \ R_{int2} \ R_{int3}] &= [2 \ 76 \ 76 \ 76] \text{ m}\Omega \\
 [b \ c \ b' \ c' \ K_{DC}] &= [230.198 \ 52.891 \ 390.9676 \ 1000 \ 325.5]
 \end{aligned}$$

The controllers shown in Fig. 6:

$$PI: (100s + 0.001)/s$$

$$PI': (0.1s + 0.1)/s$$

Time constants of low pass filters:

$$\text{in Fig. 5: } 0.001$$

$$\text{in Fig. 6: } 0.004$$

Line to line nominal voltage of transformer: 480/240 V

#### REFERENCES

- [1] M. Yilmaz and P. T. Krein, "Review of the impact of vehicle-to-grid technologies on distribution systems and utility interfaces," *Power Electronics, IEEE Transactions on*, vol. 28, no. 12, pp. 5673–5689, 2013.
- [2] —, "Review of battery charger topologies, charging power levels, and infrastructure for plug-in electric and hybrid vehicles," *Power Electronics, IEEE Transactions on*, vol. 28, no. 5, pp. 2151–2169, 2013.
- [3] K. Clement-Nyns, E. Haesen, and J. Driesen, "The impact of vehicle-to-grid on the distribution grid," *Electric Power Systems Research*, vol. 81, no. 1, pp. 185–192, 2011.
- [4] J. Rocabert, A. Luna, F. Blaabjerg, and P. Rodriguez, "Control of power converters in ac microgrids," *Power Electronics, IEEE Transactions on*, vol. 27, no. 11, pp. 4734–4749, 2012.
- [5] J. Lopes, C. Moreira, and A. Madureira, "Defining control strategies for microgrids islanded operation," *Power Systems, IEEE Transactions on*, vol. 21, no. 2, pp. 916–924, 2006.
- [6] H. Liu, Z. Hu, Y. Song, and J. Lin, "Decentralized vehicle-to-grid control for primary frequency regulation considering charging demands," *Power Systems, IEEE Transactions on*, vol. 28, no. 3, pp. 3480–3489, 2013.
- [7] M. C. Kisacikoglu, B. Ozpineci, and L. M. Tolbert, "Ev/phev bidirectional charger assessment for v2g reactive power operation," *Power Electronics, IEEE Transactions on*, vol. 28, no. 12, pp. 5717–5727, 2013.
- [8] C.-C. Hua and M.-Y. Lin, "A study of charging control of lead-acid battery for electric vehicles," in *Industrial Electronics, 2000. ISIE 2000. Proceedings of the 2000 IEEE International Symposium on*, vol. 1. IEEE, 2000, pp. 135–140.
- [9] A. A.-H. Hussein and I. Batarseh, "A review of charging algorithms for nickel and lithium battery chargers," *Vehicular Technology, IEEE Transactions on*, vol. 60, no. 3, pp. 830–838, 2011.
- [10] H. Bai and C. Mi, *Transients of Modern Power Electronics*. John Wiley & Sons, 2011.
- [11] L.-R. Chen, "Design of duty-varied voltage pulse charger for improving li-ion battery-charging response," *Industrial Electronics, IEEE Transactions on*, vol. 56, no. 2, pp. 480–487, 2009.
- [12] L.-R. Chen, N.-Y. Chu, C.-S. Wang, and R.-H. Liang, "Design of a reflex-based bidirectional converter with the energy recovery function," *Industrial Electronics, IEEE Transactions on*, vol. 55, no. 8, pp. 3022–3029, 2008.
- [13] L.-R. Chen, J.-J. Chen, C.-M. Ho, S.-L. Wu, and D.-T. Shieh, "Improvement of li-ion battery discharging performance by pulse and sinusoidal current strategies," *Industrial Electronics, IEEE Transactions on*, vol. 60, no. 12, pp. 5620–5628, 2013.
- [14] L.-R. Chen, S.-L. Wu, D.-T. Shieh, and T.-R. Chen, "Sinusoidal-ripple-current charging strategy and optimal charging frequency study for li-ion batteries," *Industrial Electronics, IEEE Transactions on*, vol. 60, no. 1, pp. 88–97, 2013.
- [15] T. Tanaka, T. Sekiya, H. Tanaka, M. Okamoto, and E. Hiraki, "Smart charger for electric vehicles with power-quality compensator on single-phase three-wire distribution feeders," *Industry Applications, IEEE Transactions on*, vol. 49, no. 6, pp. 2628–2635, 2013.
- [16] J. Pinto, V. Monteiro, H. Goncalves, and J. L. Afonso, "Onboard reconfigurable battery charger for electric vehicles with traction-to-auxiliary mode," *Vehicular Technology, IEEE Transactions on*, vol. 63, no. 3, pp. 1104–1116, 2014.
- [17] M. Kesler, M. C. Kisacikoglu, and L. M. Tolbert, "Vehicle-to-grid reactive power operation using plug-in electric vehicle bidirectional offboard charger," *Industrial Electronics, IEEE Transactions on*, vol. 61, no. 12, pp. 6778–6784, 2014.
- [18] K.-W. Hu and C.-M. Liaw, "On a bidirectional adapter with g2b charging and b2x emergency discharging functions," *Industrial Electronics, IEEE Transactions on*, vol. 61, no. 1, pp. 243–257, 2014.
- [19] A. Yazdani and R. Iravani, *Voltage-sourced converters in power systems: modeling, control, and applications*. John Wiley & Sons, 2010.